RAS-stimulated release of exosomal *miR-494-3p* promotes the osteolytic bone metastasis of breast cancer cells

OKHWA KIM[1,2*], PHUONG THAO TRAN[1*], MINJU GAL[1], SE JIN LEE[3], SUNG HUN NA[3], CHEOL HWANGBO[4] and JEONG-HYUNG LEE[1,2]

[1]Department of Biochemistry, College of Natural Sciences, Kangwon National University; [2]Kangwon Institute of Inclusive Technology, Kangwon National University; [3]Department of Obstetrics and Gynecology, Kangwon National University Hospital, School of Medicine, Kangwon National University, Chuncheon-Si, Gangwon-Do 24341; [4]Division of Applied Life Science (BK21 Four), Division of Life Science, College of Natural Sciences, Gyeongsang National University, Jinju, Gyeongsang 52828, Republic of Korea

Received March 23, 2023; Accepted July 11, 2023

DOI: 10.3892/ijmm.2023.5287

Abstract. RAS activation is a key determinant of breast cancer progression and metastasis. However, the role of the interaction among exosomes, RAS and microRNAs (miRNAs/miRs) in the osteolytic bone metastasis of breast cancer remains unclear. Therefore, the present study aimed to examine the role of activated RAS (KRAS, HRAS and NRAS) in the release of exosome-mediated osteoclastogenic miRNAs and to elucidate their functional role in bone microenvironment remodeling *in vitro* and *in vivo*. Exosomes derived from RAS-activated breast cancer cells promoted RANKL-induced osteoclastogenesis; however, RAS inhibition abolished this effect. *miR-494-3p, miR-4508* and *miR-6869-5p* were identified as osteoclastogenic miRNAs in the exosomes secreted by RAS-activated breast cancer cells. The levels of these osteoclastogenic miRNAs in the sera of patients with human epidermal growth factor receptor 2-positive luminal breast cancer were significantly higher than those in the sera of patients with triple-negative breast cancer. *miR-494-3p* exhibited both osteoclastogenic and anti-osteoblastogenic activity. Treatment with a *miR-494-3p* inhibitor abolished the exosome-mediated increase in RANKL-induced osteoclastogenesis. Treatment with a *miR-494-3p* mimic enhanced RANKL-induced osteoclast formation; however, treatment with its inhibitor suppressed this effect by targeting leucine-rich repeat-containing G-protein coupled receptor 4 in osteoclast precursors. Furthermore, *miR-494-3p* inhibited bone morphogenetic protein 2-induced osteoblast formation by targeting semaphorin 3A. In a mouse model, exosomes derived from breast cancer cells promoted osteolytic bone lesions; however, treatment with a *miR-494-3p* inhibitor significantly suppressed this effect. On the whole, the present study provides a novel mechanism, demonstrating that the RAS activation of breast cancer cells induces osteolytic bone metastasis by stimulating the exosome-mediated transfer of osteoclastogenic miRNAs, including *miR-494-3p* to bone cells.

Correspondence to: Professor Jeong-Hyung Lee, Department of Biochemistry, College of Natural Sciences, Kangwon National University, Kangwondaehak-gil 1, Chuncheon-Si, Gangwon-Do 24341, Republic of Korea
E-mail: jhlee36@kangwon.ac.kr

[*]Contributed equally

Abbreviations: ALIX, apoptosis-linked gene 2-interacting protein X; ALP, alkaline phosphatase; BMMs, bone marrow-derived macrophages; DAPI, 4',6-diamidino-2-phenylindole; ER, estrogen receptor; FEB, fetal bovine serum; GM130, Golgi matrix protein 130; HER2, human epidermal growth factor receptor 2; M-CSF, macrophage colony-stimulating factor; NTA, nanoparticle tracking analysis; PBS, phosphate-buffered saline; PR, progesterone receptor; qPCR, quantitative polymerase chain reaction; RANKL, receptor activator of nuclear factor-κB ligand; TEM, transmission electron microscopy; TRAP, tartrate-resistant acid phosphatase

Key words: breast cancer, RAS, bone metastasis, exosomes, microRNAs, osteoclast, osteoblast

Introduction

Breast cancer is the leading cause of cancer-related mortality among women globally (1,2). Bone is one of the most common target organs for breast cancer metastasis (2-5). Bone metastases are incurable and can cause skeletal-related events, including bone pain, pathological fractures, spinal cord compression and hypercalcemia, which affect the survival and quality of life in patients with advanced-stage breast cancer (2,5). Bone metastasis is the result of complex communications between tumor and stromal cells, including osteoclasts and osteoblasts, in the bone microenvironment (5-7). When breast cancer cells colonize the bone, they produce various factors that stimulate osteoclast formation and activity to induce massive bone degradation (5-7). A better understanding of the biological mechanisms through which cancer cells communicate with bone stromal cells in the bone microenvironment can lead

to the development of potential targets for the treatment or prevention of the osteolytic bone metastasis of breast cancer.

Accumulating evidence indicates that exosomes are critical mediators of intercellular communication during cancer progression and metastasis (8,9). Exosomes, also known as small extracellular vesicles, are nanosized membrane-bound vesicles surrounded by a lipid bilayer and released upon fusion of multi-vesicular bodies with the plasma membrane (10-12). Exosomes are rich in signaling molecules, including microRNAs (miRNAs/miRs), proteins, metabolites and lipids, and can deliver these signaling molecules to target cells, thereby contributing to the physiological and pathological state of target cells (11,12). Tumor-derived exosomes regulate cell proliferation and migration, angiogenesis, epithelial-mesenchymal transition and immune responses by participating in cell-cell communication in the tumor microenvironment (13,14).

RAS signaling plays a central role in the biogenesis and release of exosomes and sorting of miRNAs into exosomes in a number of types of cancer (15-17). The activation of KRAS regulates the loading of specific miRNAs into exosomes, resulting in the exosomal release of miRNAs (17,18). Oncogenic mutations in *RAS* genes (*HRAS, KRAS* and *NRAS*) are rare in human breast cancer (19). However, the hyperactivation of RAS signaling via the alternative mechanisms, including the overexpression of RAS proteins and hyperactivation of receptor tyrosine kinases, such as human epidermal growth factor receptor 2 (HER2), contributes to human breast cancer initiation and metastasis (20,21). For example, basal-like breast cancer overexpresses NRAS, which promotes tumor formation and progression (22,23), and RAS activation is a key determinant of metastasis in luminal breast cancer (21). However, the role of the interaction between RAS signaling and exosomal miRNAs in osteolytic bone metastasis of breast cancer remains unclear. Therefore, it was hypothesized that the exosomal miRNAs secreted upon the activation of RAS signaling in breast cancer cells may regulate osteoclastogenesis to promote osteolytic bone metastasis in the bone microenvironment.

The present study investigated whether the activation of RAS signaling enhances the secretion of exosomal osteoclastogenic miRNAs in human breast cancer cells. Exosomes from wild-type RAS and RAS-activated breast cancer cells were prepared, and their effects on RANKL-induced osteoclastogenesis were compared. Using a miRNA microarray, it was found that the exosomal expression levels of osteoclastogenic miRNAs, such as *miR-494-3p*, increased upon the activation of RAS signaling. The functional role of miR-494-3p in osteoclastogenesis was also investigated *in vitro* and in an animal model *in vivo*.

Materials and methods

Cells and cell culture. All the cell lines used in the present study were obtained from the American Type Culture Collection (ATCC). The MCF-7 (ATCC HTB-22) and T47D (ATCC HTB-133) cell lines are estrogen receptor (ER)-positive, progesterone receptor (PR)-positive and HER2-negative. The MDA-MB-231 (ATCC HTB-26) cell line is ER-negative, PR-negative and HER2-negative. The 4T1-Luc2 (ATCC CRL-2539-LUC2) cells are a luciferase-expressing mouse mammary carcinoma cell line. The MCF-7, T47D and 4T1-Luc2 cells were maintained in RPMI medium (cat. no. L0498-500; Biowest) supplemented with 10% fetal bovine serum (FBS; cat. no. S1480; BioWest) and 1% penicillin/streptomycin (cat. no. 15140-122; Gibco; Thermo Fisher Scientific, Inc.). The MDA-MB-231, RAW264.7 (ATCC TIB-71) murine macrophages, and C2C12 (ATCC CRL-1772) murine myoblast cell lines were cultured in DMEM (BioWest, #L0103-500) supplemented with 10% FBS and 1% penicillin/streptomycin. Bone marrow-derived macrophages (BMMs) were isolated from the tibias and femurs of 6-week-old male ICR mice (DBL Co. Ltd.), as previously described (24). The protocol was approved by the Institutional Animal Care and Use Committee (IACUC) of Kangwon National University (IACUC approval no. KW-210914-1, September 23, 2021). In brief, bone marrow cells were isolated from the femurs and tibias of ICR mice (total, six mice) and cultured in MEM (cat. no. SH30601.01; HyClone; Cytiva) containing 10% FBS, and 1% penicillin/streptomycin. Floating cells were collected and cultured for 3 days with macrophage colony-stimulating factor (M-CSF, 30 ng/ml; cat. no. cyt-439; Prospec-Tany TechnoGene, Ltd.). Cells adhering to the bottom of the culture dish were classified as BMMs. All cells were maintained at 37˚C in a humidified incubator with 5% CO_2.

Ras inhibitor, plasmids, miRNAs, siRNA and transfection. The pan-RAS inhibitor, salirasib, was purchased from MilliporeSigma (cat. no. SML1166). The *miR-494-3p* mimic (5'-UGAAACAUACACGGGAAACCUC-3', miRBase Accession no. MIMAT0002816), *miR-1915-3p* mimic (5'-CCCCAGGGCGACGCGGCGGG-3', miRBase Accession no. MIMAT0007892), *miR-4508* mimic (5'-GCGGGGCUGGGCGCGCG-3', miRBase Accession no. MIMAT0019045), *miR-4516* mimic (5'-GGGAGAAGG GUCGGGGC-3', miRBase Accession no. MIMAT0019053), *miR-6088* mimic (5'-AGAGAUGAAGCGGGGGGGCG-3', miRBase Accession no. MIMAT0023713), *miR-6869-5p* mimic (5'-GUGAGUAGUGGCGCGCGGCGGC-3', miRBase Accession no. MIMAT0027638), *miR-494-3p* inhibitor (5'-ACUUUGUAUGUGCCCUUUGGAG-3'), miRNA mimic negative control (cat. no. SMC-2003), and miRNA inhibitor negative control (cat. no. SMC-2103) were all purchased from Bioneer Corporation. The pMT3-HRASV12, pMT3-NRASV12 and pMT3-KRASV12 constructs were kindly provided by Professor Lee Kwang-Yeol (Cheonnam National University, Kwangju, Korea). The HER2 expression vector (cat. no. HG10004-UT) was purchased from Sino Biological. The control siRNA (cat. no. sc-37007) and siRNA for leucine-rich repeat-containing G-protein coupled receptor 4 (*LGR4*; cat. no. sc-62558) were purchased from Santa Cruz Biotechnology, Inc. The cells were seeded in a cell culture dish ($2.5x10^5$ cells/ml), cultured for 24 h, and then transfected with nucleic acids (plasmids, 1 μg per transfection; siRNAs or miRNAs, 10 or 100 μM) using Lipofectamine 3000 (for plasmids, cat. no. L3000-015) or RNAiMAX (for siRNAs and miRNAs, cat. no. 13778-150) according to the manufacturer's instructions (Thermo Fisher Scientific, Inc.) After 48 h, the transfected cells were used for further experiments.

miRNA microarray. Exosomes isolated from the MCF-7 cells transfected with control or *KRASV12* were used for miRNA microarray analysis by Macrogen Inc. The miRNA microarray system with Affymetrix GeneChip® 4.0 array (Affymetrix; Thermo Fisher Scientific, Inc.) containing 2,578 human mature miRNA oligonucleotide probes was used according to the manufacturer's recommended protocol (Affymetrix; Thermo Fisher Scientific, Inc.). Raw data were extracted in the Affymetrix data extraction protocol using the software provided by Affymetrix GeneChip® Command Console® Software. The CEL files import, miRNA level RMA+DABG-All analysis and result export were conducted using Affymetrix® Power Tools Software. Array data were filtered using probes for annotated species. Comparative analysis between the control and test samples was carried out using fold changes. For a significant DEmiRNA set, hierarchical cluster analysis was performed using complete linkage and Euclidean distance as measures of similarity. All statistical tests and visualization of differentially expressed genes were performed using the R statistical language v. 3.3.2 (https://www.r-project.org).

In vitro osteoclastogenesis and bone resorption assays. BMMs transfected with the indicated miRNAs were plated in 96-wells plate at a density of $5x10^5$ cells/ml and then stimulated with M-CSF (30 ng/ml; cat. no. cyt-439; Prospec-Tany TechnoGene, Ltd.) and receptor activator of nuclear factor-κB ligand (RANKL, 100 ng/ml; cat. no. 462-TEC-010; R&D Systems, Inc.) for 6 days with a change in medium every 2 days. The RAW264.7 cells ($5x10^4$ cells/ml) were seeded in a 96-well plate and stimulated with RANKL (100 ng/ml) for 4 days with a change in medium every 2 days. At the end of the incubation (6 days for BMMs, 4 days for RAW264.7 cells) at 37˚C, the tartrate-resistant acid phosphatase (TRAP) staining of osteoclasts was performed using a leukocyte acid phosphatase staining kit (cat. no. 387A; MilliporeSigma). TRAP-positive multinucleated cells with more than five nuclei were quantified as mature osteoclasts. For the bone resorption assay, BMMs transfected with the indicated miRNAs were cultured in OsteoAssay Surface 96-well plates (cat. no. 3989; Corning, Inc.) and primed with M-CSF and RANKL as described above. After 6-7 days, the cells were removed from the wells with sodium hypochlorite solution and washed with distilled water. Resorption pits were captured using a model H550L microscope (Nikon Corporation) and quantified using ImageJ software [Java 1.6.0_20 (64 bit); National Institutes of Health].

Alkaline phosphatase (ALP) activity. To induce osteoblast differentiation, the C2C12 cells (10^5 cells/ml) were seeded in a 48-well plate. Upon reaching confluency, the cells were transfected with the indicated miRNAs and stimulated with bone morphogenetic protein 2 (BMP2; 30 ng/ml, cat. no. 355-BM; R&D Systems, Inc.) for 3 days. ALP activity assay was performed following the manufacturer's instructions (cat. no. MAK447; MilliporeSigma).

Immunofluorescence staining and confocal microscopy. The cells were washed with phosphate-buffered saline (PBS), fixed in 4% paraformaldehyde for 10 min at 25˚C and permeabilized in 0.1% Triton X-100 for 30 min. After being washed with PBS, the cells on the glass coverslips were incubated with anti-nuclear factor of activated T-cells (NFATc1; dilution, 1:500; cat. no. 8032; Cell Signaling Technology, Inc.) or RelA/p65 (dilution, 1:500; cat. no ; sc8008; Santa Cruz Biotechnology, Inc.) antibodies at 4˚C overnight, and washed with PBS three times. The cells were then incubated with anti-rabbit secondary Alexa (dilution, 1:500; cat. no. A11008, Thermo Fisher Scientific, Inc.) or anti-mouse secondary Alexa 488 antibody (dilution, 1:500; cat. no. A11001, Thermo Fisher Scientific, Inc.) for 4 h at room temperature. Cell nuclei were counterstained with 4',6-diamidino-2-phenylindole (DAPI; cat. no. D9542; MilliporeSigma) for 5 min at room temperature and mounted with a mounting solution (cat. no. M01; Biomeda Corp.). Confocal images were acquired using a confocal laser microscope (LSM 880; Airyscan, Carl Zeiss AG).

Western blot analysis and antibodies. Cells and exosomes were lysed in lysis buffer [50 mM Tris-HCl (pH 7.4), 1 mM ethylenediaminetetraacetic acid (EDTA), 1% NP 40, 150 mM sodium chloride, 5 mM sodium orthovanadate and protease inhibitor cocktail; cat. no. 11836145010, Roche; MilliporeSigma], and centrifuged at 20,000 x g for 15 min at 4˚C. The lysates (30 μg/sample) were loaded equally and separated using 8-12% sodium dodecyl sulfate-polyacrylamide gel electrophoresis. The proteins on the gel were then transferred to a Hybond-P membrane (cat. no. 10600023; Cytiva), followed by incubation with blocking solution (PBS containing 5% skim milk or BSA) for 4 h at room temperature. The membrane was then incubated with primary antibody with shaking at 4˚C overnight. After being washed with PBS containing tween-20 (cat. no. P7949; Sigma-Aldrich), the membrane was probed with the appropriate secondary antibody conjugated to horseradish peroxidase. The primary and secondary antibodies used in the present study are listed in Table SI. The protein signal was observed using an enhanced chemiluminescence system (cat. no. LR 01-01; BioNote).

Exosome isolation, nanoparticle tracking analysis (NTA) and transmission electron microscopy (TEM). Exosomes were collected from the cell culture supernatant using differential ultracentrifugation, as previously described (25). The culture supernatant was centrifuged at 300 x g for 15 min at 4˚C to remove cellular debris and subsequently centrifuged at 10,000 x g for 30 min at 4˚C. The supernatant was centrifuged at 100,000 x g for 70 min at 4˚C using an Optimal LE-80K ultracentrifuge (SW55Ti rotor, Beckman Coulter, Inc.). The pellet was resuspended in PBS and centrifuged at 100,000 x g for 70 min at 4˚C. The supernatant was discarded, and the precipitated exosomes were used for further experiments. The size distribution and concentration of exosomes were analyzed using NTA with NanoSight NS300 (Malvern Panalytical, Ltd.) as previously described (25). TEM was performed to observe the morphology of purified exosomes, as previously described (25). The suspension (20 μl) was applied to a carbon-coated grid that was previously glow-discharged (Harrick Plasma, Inc.) for 3 min in air, followed by negative staining with 2% uranyl acetate. The prepared grids were identified using TEM on a JEM 2100F microscope (JEOL) operating at 200 kV. Images were acquired using a one view camera (Gatan, Inc.).

In vitro exosome uptake assay. The purified exosomes were labeled with PKH26 according to the manufacturer's protocol (cat. no. PKH26GL-1KT; MilliporeSigma). PKH26 was added to exosomes in a total volume of 400 μl of diluent C and the mixture was incubated for 5 min at 37˚C. The labeling reaction was terminated by the addition of an equal volume of 1% BSA. The labeled exosomes were collected using ultracentrifugation at 100,000 x g for 70 min at 4˚C. The supernatant was removed, and the pellet was resuspended in 50 μl PBS. The BMMs and RAW264.7 cells cultured on glass coverslips for 24 h were incubated with PKH26-labeled exosomes for 12 h at 37˚C with 5% CO_2. At the end of the incubation period, the cells were washed with PBS, fixed with 4% paraformaldehyde for 10 min at room temperature and then mounted with a mounting solution. Images were captured using a confocal laser 21 microscope (LSM 880 with Airyscan, Carl Zeiss AG).

Reverse transcription-quantitative PCR (RT-qPCR). Total RNA was isolated using TRIzol reagent according to the manufacturer's instructions (cat. no. FATRR001; Favorgen Biotech Corp.). For the analysis of mRNA expression, total RNA was reverse transcribed into cDNA using the Maxime RT PreMix kit (cat. no. 25081; Intron Biotechnology, Inc.). For the analysis of miRNA expression, cDNA was synthesized using the miScript II RT kit (cat. no. 218161; Qiagen, Inc.). Quantitative PCR (qPCR) was performed on StepOne Real-time PCR System (Applied Biosystems; Thermo Fisher Scientific, Inc.) using 2X Fast Q-PCR Mastermix (cat. no. TG1210; SMOBIO Technology, Inc.). The optimized qPCR conditions were as follows: 95˚C for 20 sec, followed by 40 cycles at 95˚C for 10 sec, 55˚C for 10 sec, and 72˚C for 20 sec. *GAPDH* was used as a normalization control for mRNA expression in cells. U6 small nuclear RNA (*RNU6-1*) was used as a normalization control for miRNA expression in the cells and exosomes. All the primer sequences used in the present study are listed in Tables SII and SIII. The qPCR reverse primer for all miRNAs including U6 used was the universal reverse primer provided with the kit (cat. no. 218161; Qiagen, Inc.).

Blood samples and analysis of miRNA expression in serum. Blood samples from Korean patients with a confirmed diagnoses of ductal carcinoma (n=19) and triple-negative breast cancer (n=15) were collected at Kangwon National University Hospital (Chuncheon, Korea). The present study was performed following the guiding principles of the Declaration of Helsinki. In addition, it was approved by the Institutional Review Board of Kangwon National University Hospital (approval no. KNUH-2022-04-011, approval date, May 4, 2022). The requirement for informed consent was waived by the Institutional Review Board of Kangwon National University Hospital owing to the retrospective nature of the study. The clinicopathological characteristics of the breast tumor tissues from the patients are presented in Table SIV. Blood in containers was kept at 4˚C for 4 h to ensure serum separation. Serum samples were centrifuged at 1,000 x g for 10 min and stored at -80˚C until use. RNA was extracted from serum using TRIzol reagent according to the manufacturer's protocol (cat. no. FATRR001; Favorgen Biotech Corp.). The expression levels of miRNAs were determined using qPCR, as described above. U6 small nuclear RNA (*RNU6-1)* was used as a normalization control for miRNA expression in serum.

Animal experiment. Female BALB/c mice (6 weeks old; n=24; weight, 18.5-20.3 g) were purchased from DBL Co., Ltd. All experimental protocols were approved by the Institutional Animal Care and Use Committee (IACUC) of Kangwon National University (IACUC approval no. KW-210914-1, September 23, 2021). The mice were housed under standard laboratory conditions (light cycle, 12 h dark/12 h light; temperature, 22±2˚C; humidity, 55±2.5%), and were provided with *ad libitum* access to food and water. For intratibial injection, the mice were anesthetized by an intraperitoneal injection of 100 mg/kg ketamine and 10 mg/kg xylazine. To mimic established breast cancer bone metastases, the mice (n=24) were treated with exosomes derived from 4T1-Luc2 cells (10^9 particles/mouse) by tail vein injection once a day. After 14 days, $1x10^5$ 4T1-Luc2 cells in 10 μl sterile PBS were injected once into the intratibial bone marrow cavity of the mice. The mice were then randomly assigned to three groups (n=8 in each group) as follows: The control group treated with PBS plus negative control (NC) miRNA (0.06 nmol/mouse); the exosome group treated with exosomes derived from 4T1-Luc2 cells (10^9 particles/mouse) plus NC (0.06 nmol/mouse); and the exosome plus inhibitor (IN) group treated with exosomes derived from 4T1-Luc2 cells (10^9 particles/mouse) plus *miR-494-3p* IN (0.06 nmol/mouse). Subsequently, the mice were administered PBS plus NC, exosomes plus NC, or exosomes plus IN intravenously via the tail vein three times a week (at 2- to 3-day intervals) for 2 weeks. The NC and IN were incubated with exosomes for 30 min at room temperature prior to the tail vein injection. Tumor growth in the tibia was measured using bioluminescent imaging with Spectral Instruments Imaging following the intraperitoneal injection of 150 mg/kg sterile d-luciferin (cat. no. P1042; Promega Corporation). All experimental animals were monitored once every 2 days, and if they lost food or water intake, activity, or weight, they were euthanized. The euthanasia of animals progressed to cervical dislocation following an anesthetic injection (100 mg/kg ketamine and 10 mg/kg xylazine). Tibiae were collected at the end of the experiment. For histological analysis, the tibiae were fixed in 4% paraformaldehyde for 1 day at room temperature, decalcified in 12% EDTA for 3 weeks, and embedded in paraffin. Sections of 7 μm thickness were prepared and stained with hematoxylin (cat. no. HHS16; Sigma-Aldrich) and eosin (cat. no. E4009) for 1 min at room temperature, and TRAP for 1 h at 37˚C. The stained sections were scanned using the Grundium Ocus scanner (Grandium).

Statistical analysis. Data are expressed as the mean ± standard deviation (SD). Statistical analyses to determine the significance between groups were performed using one-way analysis of variance (for comparisons of more than two groups) followed by Tukey's multiple comparisons test or an unpaired Student's t-test (for comparisons between two groups). All statistical analyses were performed using GraphPad Prism 9 software (Dotmatics). A P-value ≤0.05 was considered to indicate a statistically significant difference.

Results

Exosomes derived from RAS-activated breast cancer cells stimulate RANKL-induced osteoclast formation in vitro. First, to investigate the role of RAS activation in the exosome-mediated osteolytic bone metastases of breast cancer cells, the *KRAS* mutant MDA-MD-231 cell line was used, which forms osteolytic bone metastases, as a model system. Exosomes from MDA-MB-231 cells were isolated and analyzed for their physical features and the expression of marker proteins. TEM analysis revealed that exosomes purified from MDA-MB-231 cells had a typical exosome morphology, exhibiting round and cup shapes with sizes ranging from 50 to 150 nm (Fig. 1A). In addition, NTA revealed that the average size of the exosomes was 109.9±3.6 nm (Fig. 1B), indicating that most of the exosomes isolated from MDA-MB-231 cells were distributed within the range of the exosome diameter. Exosomal markers, including apoptosis-linked gene 2-interacting protein X (ALIX), tumor susceptibility gene 101 (TSG101) and syntenin-1, were detected; however, Golgi matrix protein 130 (GM130), a Golgi marker, was not detected in the exosomes isolated from the MDA-MB-231 cells (Fig. 1C), suggesting that the exosomes were successfully isolated from the MDA-MB-231 cells.

Subsequently, the present study determined whether exosomes derived from the MDA-MB-231 cells stimulated RANKL-induced osteoclast formation. Treatment of the BMMs with exosomes derived from MDA-MB-231 cells significantly increased the number of TRAP-positive multinucleated osteoclasts (Fig. 1D). By contrast, treatment with exosomes derived from the MDA-MB-231 cells treated with the pan RAS inhibitor, salirasib, significantly decreased the number of TRAP-positive osteoclasts, compared with that in the control group (Fig. 1E). To investigate whether the activation of RAS signaling contributes to exosome-mediated osteoclastogenesis, the MCF-7 and T47D cell lines, which carry wild-type RAS and do not overexpress HER2, were transfected with mutant RAS or HER2. Transfection of the MCF-7 cells with KRASV12 increased the expression levels of pan-RAS and p-ERK (Fig. S1A). Treatment of the BMMs with exosomes derived from MCF-7 cells transfected with a KRASV12 expression vector (MCF-7/KRASV12) significantly promoted RANKL-induced osteoclastogenesis compared with the exosomes derived from the MCF-7 cells transfected with a control vector (MCF-7/Con MCF-7/Con cells) (Fig. 1F). In addition, the effect of RAS signaling on exosome-mediated osteoclastogenesis in T47D cells following the overexpression of *KRASV12*, *HRASV12*, *NRASV12*, or *HER2* was also determined (Fig. S1B and C). Exosomes derived from T47D cells transfected with *KRASV12*, *HRASV12*, *NRASV12*, or *HER2* stimulated RANKL-induced osteoclastogenesis (Fig. 1G and H). NTA revealed that the enforced expression of *KRASV12*, *HRASV12*, or *NRASV12* in the MCF-7 or T47D cells increased the concentration of exosomes (Fig. S1D and E). Moreover, the transfection of *HER2* into the T47D cells also increased the concentration of exosomes (Fig. S1F). By contrast, treatment of the MDA-MB-231 cells with salirasib decreased the concentration of exosomes (Fig. S1G). These results indicated that RAS activation stimulated exosome-mediated osteoclastogenesis by regulating the release of exosomes and/or loading cargo into exosomes in breast cancer cells.

Identification of RAS-dependent osteoclastogenic miRNAs in exosomes. To identify miRNAs that could be loaded into exosomes via RAS activation, miRNA expression profiles were compared between exosomes derived from MCF-7/KRASV12 and MCF-7/Con cells using a miRNA microarray. A total of 23 miRNAs were upregulated, and five miRNAs were downregulated in the exosomes derived from the MCF-7/KRASV12 cells (Fig. S2A-C). To confirm the expression of these 28 miRNAs in exosomes, their expression levels in exosomes were analyzed using RT-qPCR. In total, 11 miRNAs whose expression levels were high were selected, and their expression levels in exosomes derived from the MCF-7/KRASV12 and MCF-7/Con cells were compared (Fig. 2A and B). The levels of eight miRNAs among these were significantly increased in the exosomes derived from the MCF-7/KRASV12 cells compared to the exosomes from the MCF-7/Con cells (Fig. 2B). However, the cellular expression levels of these miRNAs were not significantly increased by KRASV12 (Fig. 2C). Treatment of the MDA-MB-231 cells with salirasib significantly decreased the levels of seven miRNAs in exosomes (Fig. 2D). Moreover, the transfection of NRASV12 into the T47D cells increased the expression levels of six miRNAs (*miR-494-3p, miR-1915-3p, miR-4508, miR-4516, miR-6088* and *miR-6869-5p*) in exosomes, apart from *miR-4530* (Fig. 2E), suggesting that RAS activation increased the loading of these miRNAs into exosomes.

Subsequently, the effects of these six miRNAs on RANKL-induced osteoclastogenesis in BMMs and BMP2-induced osteoblastogenesis in C2C12 cells were determined. Transfection of these miRNA mimics into BMMs significantly increased their expression levels (Fig. S2D). Three miRNAs (*miR-494-3p, miR-4508* and *miR-6869-5p*) significantly promoted RANKL-induced osteoclast formation in BMMs (Fig. 2F), and two miRNAs (*miR-494-3p* and *miR-1915-3p*) significantly suppressed BMP2-induced osteoblastogenesis (Fig. S2E). The present study also determined the expression levels of these four miRNAs in the serum of patients with HER2-positive and triple-negative breast cancer. The levels of *miR-494-3p, miR-1915-3p, miR-4508* and *miR-6869-5p* in serum from patients with HER2-positive breast cancer were significantly higher than those in the serum of patients with triple-negative breast cancer (Fig. 2G). Therefore, *miR-494-3p* was selected for further analyses based on its RAS-dependent expression in exosomes and potent regulatory effects on osteoclastogenesis and osteoblastogenesis.

miR-494-3p in exosomes derived from breast cancer cells is taken up into osteoclast precursors, and promotes RANKL-induced osteoclastogenesis. PKH-labeled exosomes derived from the MDA-MB-231 cells were internalized into BMMs and RAW264.7 cells (Fig. 3A) and treatment of the BMMs with exosomes derived from the MDA-MB-231 cells significantly increased the expression of *miR-494-3p* in BMMs (Fig. 3B), indicating that exosomes derived from the MDA-MB-231 cells were effectively taken up by osteoclast precursors. Treatment of the BMMs with exosomes significantly increased the number of TRAP-positive osteoclasts, whereas treatment with *miR-494-3p* inhibitor inhibited the exosome-mediated increase in osteoclast formation (Fig. 3C). The functional role of *miR-494-3p* in RANKL-induced osteoclastogenesis was then examined.

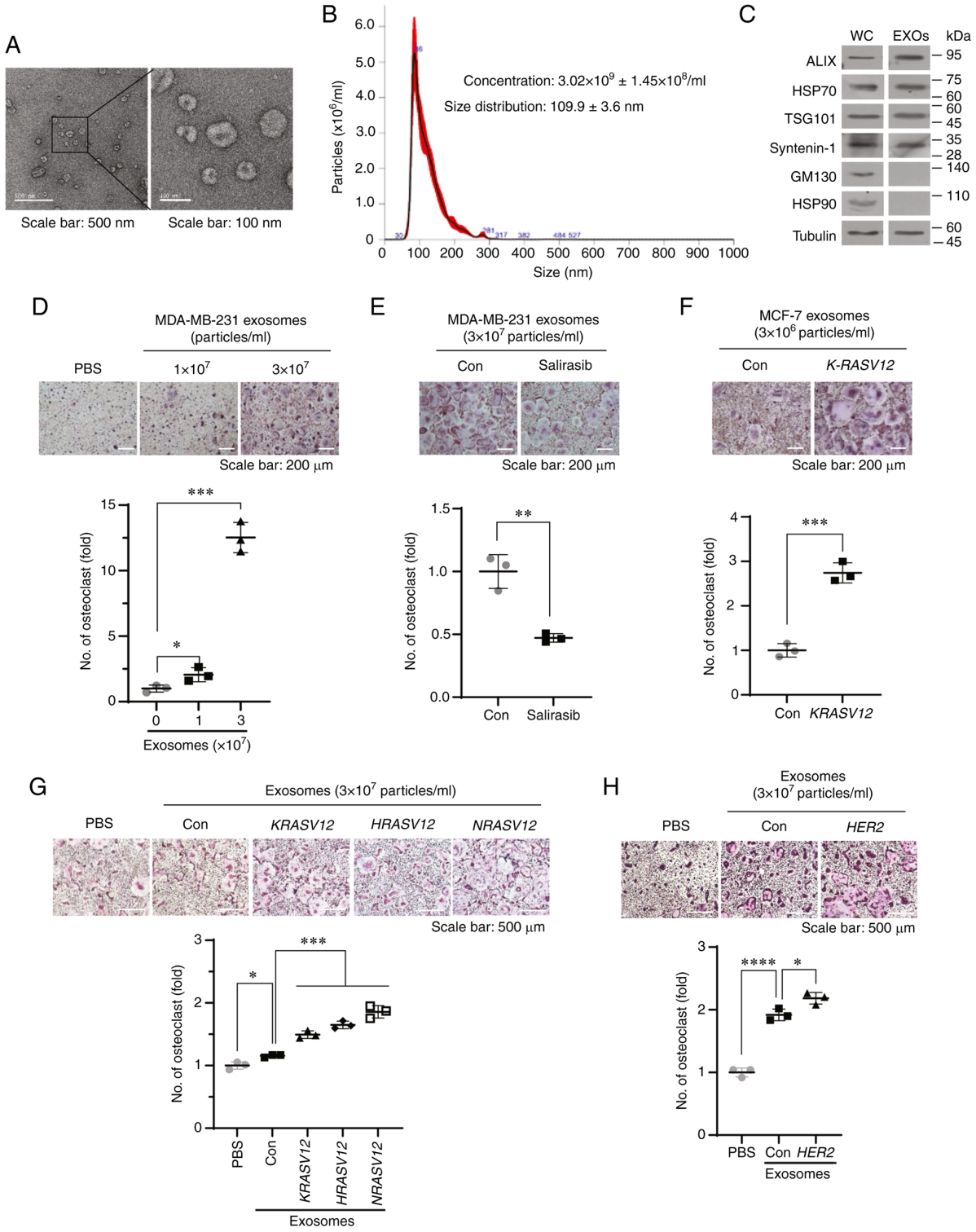

Figure 1. Exosomes derived from MDA-MB-231 cells stimulate RANKL-induced osteoclastogenesis *in vitro*. (A) Representative transmission electron microscopy images of exosomes derived from MDA-MB-231 cells. Scale bar, 500 nm (left panel) and 100 nm (right panel). (B) Nanoparticle tracking analysis of exosomes derived from MDA-MB-231 cells. (C) Western blot analysis of whole cell lysates (WC) and exosomes (EXOs) prepared from MDA-MB-231 cells. (D) BMMs were treated with exosomes derived from MDA-MB-231 cells in the presence of RANKL and M-CSF for 4 days. Representative TRAP staining images and quantification of TRAP-positive multinucleated cells. *P<0.05 and ***P<0.001. (E) BMMs were treated with exosomes derived from MDA-MB-231 cells treated with vehicle (Con) or the pan RAS inhibitor, salirasib (10 μM), in the presence of RANKL and M-CSF for 6 days. Representative TRAP staining images and quantification of TRAP-positive multinucleated cells. **P<0.01. (F) BMMs were treated with exosomes derived from MCF-7 cells transfected with control vector (Con) or K-RASV12 vector in the presence of RANKL and M-CSF for 6 days. Representative TRAP staining images and number of TRAP-positive multinucleated cells. ***P<0.001. (G) BMMs were treated with exosomes derived from T47D cells transfected with control vector (Con), *K-RASV12*, *H-RASV12*, or *N-RASV12* vector in the presence of RANKL and M-CSF for 6 days. Representative TRAP staining images and number of TRAP-positive multinucleated cells. *P<0.05 and ***P<0.001. (H) BMMs were treated with exosomes derived from control vector (Con) or HER2 vector-transfected T47D cells in the presence of RANKL and M-CSF for 6 days. *P<0.05 and ****P<0.0001. RANKL, receptor activator of nuclear factor-κB ligand; BMMs, bone marrow-derived macrophages; TRAP, tartrate-resistant acid phosphatase; M-CSF, macrophage colony-stimulating factor; EXOs, exosomes; ALIX, apoptosis-linked gene 2-interacting protein X; HSP, heat shock protein; TSG101, tumor susceptibility 101; GM130, Golgi matrix protein 130; HER2, human epidermal growth factor receptor 2.

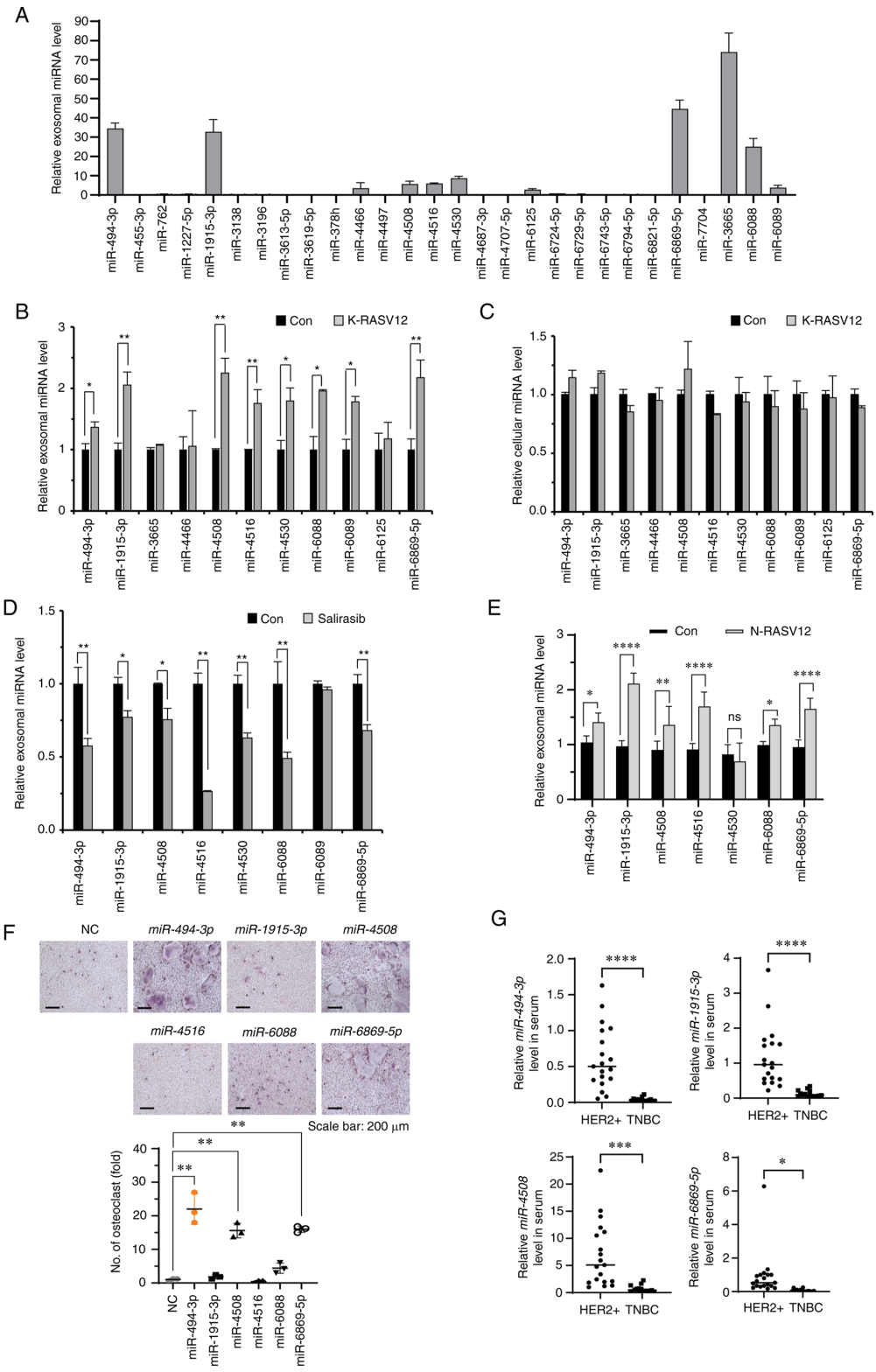

Figure 2. Identification of osteoclastogenic miRNAs in exosomes induced by RAS activation. (A) Expression levels of 28 miRNAs in exosomes derived from MCF-7 cells were determined using RT-qPCR. The results were normalized to U6 snRNA. (B) The expression levels of 11 selected miRNAs in exosomes derived from control or KRASV12 vector-transfected MCF-7 cells were determined using RT-qPCR. The results were normalized to U6 snRNA. *P<0.05 and **P<0.01. (C) Cellular expression levels of 11 selected miRNAs in MCF-7 cells transfected with the control or K-RASV12 vector were determined using RT-qPCR. The results were normalized to U6 snRNA. (D) The expression levels of eight selected miRNAs in exosomes derived from MDA-MB-231 cells treated with the control or salirasib (10 μM) were determined using RT-qPCR. The results were normalized to U6 snRNA. *P<0.05 and **P<0.01. (E) The expression levels of seven selected miRNAs in exosomes derived from T47D cells transfected with the control vector (Con) or N-RASV12 vector were determined using RT-qPCR. The results were normalized to U6 snRNA. *P<0.05, **P<0.01 and ****P<0.0001. (F) Representative images of TRAP-positive osteoclasts in BMMs transfected with the indicated miRNAs. BMMs transfected with the indicated miRNAs (20 nM each) were stimulated with RANKL and M-CSF for 4 days. NC, miRNA mimic negative control. **P<0.01. (G) The expression levels of *miR-494-3p, miR-1915-3p, miR-4508* and *miR-6869-5p* in sera derived from patients with HER2-positive breast cancer (n=19) and triple-negative breast cancer (n=15). The results were normalized to U6 snRNA. *P<0.05, ***P<0.001 and ****P<0.0001. RT-qPCR, reverse transcription-quantitative PCR; M-CSF, macrophage colony-stimulating factor; HER2, human epidermal growth factor receptor 2; TNBC, triple-negative breast cancer; BMMs, bone marrow-derived macrophages.

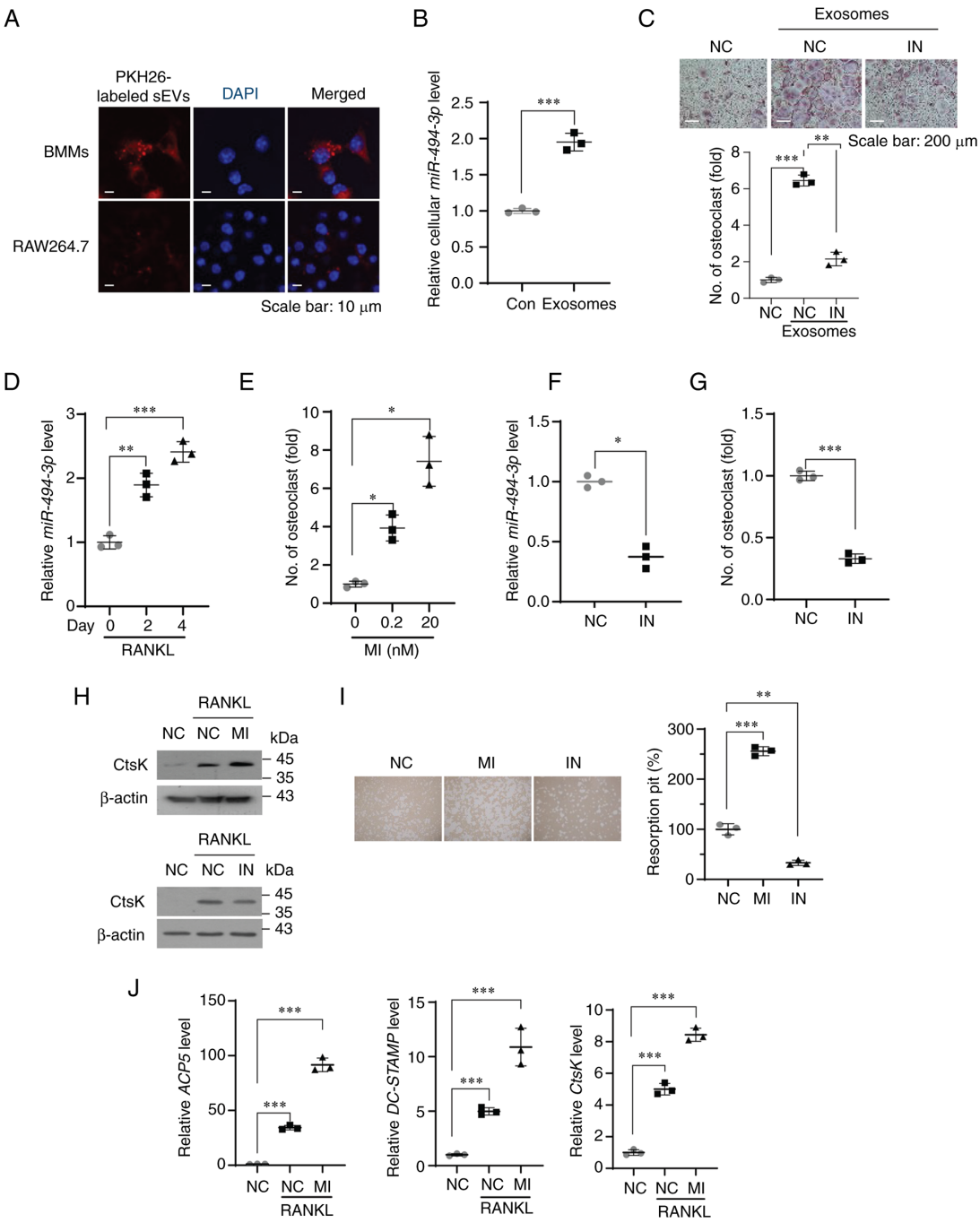

Figure 3. miR-494-3p in exosomes derived from breast cancer cells stimulates RANKL-induced osteoclast differentiation. (A) Representative confocal microscopy images of BMMs (upper panels) and RAW264.7 cells (lower panels) treated with PKH26-labeled exosomes derived from MDA-MB-231 cells for 24 h. Cell nuclei were stained with DAPI (blue). (B) Expression level of *miR-494-3p* in BMMs treated with PBS (Con) and exosomes (3x107 particles/ml) derived from MDA-MB-231cells for 24 h was determined using RT-qPCR (n=3). ***P<0.001. (C) BMMs were transfected with miRNA inhibitor negative control miRNA (NC) or miR-494-3p inhibitor (IN, 100 nM) and sunsequently stimulated with exosomes (3x107 particles/ml) derived from MDA-MB-231 cells in the presence of M-CSF and RANKL for 5 days. Representative image of TRAP staining. Graph represents the number of TRAP-positive multinucleated osteoclasts (n=3). Scale bar, 200 μm. **P<0.01 and ***P<0.001. (D) BMMs were stimulated with RANKL and M-CSF for the indicated period. Expression level of miR-494-3p was determined using RT-qPCR (n=3). The results were normalized to U6 snRNA. **P<0.01 and ***P<0.001. (E) BMMs were transfected with miRNA mimic negative control (NC) and *miR-494-3p* mimic (MI, 0.2 and 20 nM) in the presence of M-CSF and RANKL for 5 days. The graph represents the number of TRAP-positive multinucleated osteoclasts (n=3). *P<0.05. (F) BMMs were transfected with miRNA inhibitor negative control (NC) and miR-494-3p inhibitor (IN, 100 nM). The expression level of miR-494-3p in BMMs was determined using RT-qPCR (n=3). The results were normalized to U6 snRNA. *P<0.05. (G) BMMs were transfected with miRNA inhibitor negative control (NC) and miR-494-3p inhibitor (IN, 100 nM) in the presence of M-CSF and RANKL for 5 days. The graph represents the number of TRAP-positive multinucleated osteoclasts (n=3). ***P<0.001. (H) BMMs transfected with negative control miRNA, *miR-494-3p* mimic (MI, 20 nM), or miR-494-3p inhibitor (IN, 100 nM) were stimulated with RANKL and M-CSF for 4 days. Western blot analysis was performed to determine the expression levels of CtsK and β-actin. (I) BMMs transfected with negative control miRNA, *miR-494-3p* mimic (MI, 20 nM), or *miR-494-3p* inhibitor (IN, 100 nM) were stimulated with M-CSF and RANKL for 6 days. Pit resorption area was measured using ImageJ software (n=3). **P<0.01 and ***P<0.001. (J) BMMs were transfected with miRNA mimic negative control (NC) or miR-494-3p mimic (MI, 20 nM) and subsequently stimulated with M-CSF and RANKL for 6 days. RT-qPCR was performed to determine the mRNA expression levels of *CtsK, ACP5* and *DC-STAMP* (n=3). ***P<0.001. RT-qPCR, reverse transcription-quantitative PCR; RANKL, receptor activator of nuclear factor-κB ligand; BMMs, bone marrow-derived macrophages; TRAP, tartrate-resistant acid phosphatase; M-CSF, macrophage colony-stimulating factor; CtsK, cathepsin K; ACP5, acid phosphatase 5, tartrate resistant; DC-STAMP, dendrocyte expressed seven transmembrane protein.

Stimulation of the BMMs with RANKL increased the expression of *miR-494-3p* (Fig. 3D), and treatment with *miR-494-3p* mimic promoted formation of TRAP-positive osteoclasts (Fig. 3E). In contrast, treatment with *miR-494-3p* inhibitor decreased the expression of *miR-494-3p* (Fig. 3F) and inhibited RANKL-induced osteoclastogenesis (Fig. 3G). Treatment with *miR-494-3p* mimic increased the expression of CtsK, an osteoclast marker, and the formation of resorption pits by mature osteoclasts in response to RANKL, whereas treatment with *miR-494-3p* inhibitor suppressed these effects (Fig. 3H and I). Moreover, treatment with *miR-494-3p* mimic increased the RANKL-induced expression of NFATc1 target genes, including ACP5, acid phosphatase 5, tartrate resistant (*ACP5*), cathepsins K (*CtsK*) and dendrocyte expressed seven transmembrane protein (*DC-STAMP*) (Fig. 3J). These results suggested that *miR-494-3p* may be a positive regulator of RANKL-induced osteoclastogenesis in BMMs and exosomes derived from breast cancer cells stimulated osteoclast differentiation, at least in part, by transferring exosomal *miR-494-3p* to osteoclast precursors.

LGR4 is a potential target of miR-494-3p in osteoclast precursors. To elucidate the molecular mechanisms by which *miR-494-3p* regulates osteoclast differentiation, potential target genes of *miR-494-3p* were analyzed using two most widely used miRNA target prediction databases: miRDB (mirdb.org) and TargetScan (targetscan.org). *LGR4*, a negative regulator of osteoclast differentiation (26), was identified as a potential target gene of *miR-494-3p* in osteoclast precursors (Fig. 4A). Treatment with *miR-494-3p* mimic significantly suppressed both the mRNA and protein expression of LGR4, whereas treatment with *miR-494-3p* inhibitor markedly increased the mRNA and protein expression of LGR4 (Fig. 4B and C). Consistent with the LGR4 expression levels, treatment with *miR-494-3p* inhibitor decreased the expression of *miR-494-3p*, whereas treatment with *miR-494-3p* mimic increased the expression of *miR-494-3p* in RAW264.7 cells (Fig. S3A). Treatment of the RAW264.7 cells with exosomes derived from the MDA-MB-231 cells resulted in a significant decrease in the protein expression of LGR4; however, treatment with *miR-494-3p* inhibitor reversed the exosome-mediated downregulation of LGR4 (Fig. 4D).

LGR4 is a receptor for RANKL and negatively regulates RANKL-induced osteoclast differentiation by inhibiting the RANKL-induced activation of NF-κB and NFATc1 (26). RANKL binding to LGR4 activates Gq protein α-subunit, resulting in the inhibition of the glycogen synthase kinase (GSK)-3b-mediated activation of NFATc1 (26). Thus, the present study then determined the effects of *miR-494-3p* on the RANKL-induced activation of NF-κB and NFATc1. Treatment with *miR-494-3p* inhibitor significantly blocked the RANKL-induced degradation of IκBα and the nuclear translocation of the RelA/p65 subunit of NF-κB (Fig. S3B and C). In addition, *miR-494-3p* inhibitor blocked the RANKL-induced nuclear translocation and dephosphorylation of NFATc1 (Fig. 4E and F) and GSK-3β phosphorylation (Fig. 4G). *LGR4* knockdown markedly increased the RANKL-induced expression of NFATc1 target genes, including *CtsK*, *ACP5*, *DC-STAMP* and *MMP-9* (Figs. 4H and S3D), whereas treatment with *miR-494-3p* inhibitor impaired these effects (Fig. 4H). Overall, these findings suggest that *miR-494-3p* in exosomes stimulates RANKL-induced osteoclastogenesis by downregulating the expression of LGR4 in osteoclast precursors.

miR-494-3p inhibits osteoblastogenesis by targeting semaphorin 3A (SEMA3A). *SEMA3A* was also identified as a potential target of *miR-494-3p* (Fig. 5A). SEMA3A stimulates osteoblast differentiation and inhibits osteoclast differentiation (27). As osteoblasts mainly express SEMA3A (27,28), the present study then investigated whether *miR-494-3p* regulates BMP2-induced osteoclastogenesis by targeting *SEMA3A* in C2C12 cells. Treatment of the C2C12 cells with *miR-494-3p* mimic or *miR-494-3p* inhibitor effectively modulated decreased the expression level of *miR-494-3p* (Fig. S4A and B). Treatment with *miR-494-3p* mimic decreased the protein and mRNA expression of SEMA3A, whereas treatment with *miR-494-3p* inhibitor increased the expression of SEMA3A in C2C12 cells (Fig. 5B and C). Treatment of the C2C12 cells with exosomes derived from MDA-MB-231 cells decreased the protein and mRNA expression levels of SEMA3A (Fig. 5D and E). The expression of *miR-494-3p* was downregulated by treatment with BMP2 in C2C12 cells (Fig. 5F). Treatment of the C2C12 cells with exosomes derived from the MDA-MB-231 cells reduced BMB2-induced osteoblast formation (Fig. 5G). Moreover, treatment with *miR-494-3p* mimic suppressed BMP2-induced osteoblastogenesis, whereas treatment with *miR-494-3p* inhibitor reversed this effect (Fig. 5H). On the whole, these results indicated that *miR-494-3p* in exosomes impaired BMP2-induced osteoblastogenesis by targeting *SEMA3A*.

Exosomes stimulate tumor growth in the tibia, whereas treatment with miR-494-3p inhibitor suppresses it. Mouse 4T1-Luc2 cell-derived exosomes abundantly expressed *miR-494-3p* and stimulated RANKL-induced osteoclast formation (Fig. 6A and B). Thus, the present study then investigated whether 4T1-Luc2 cell-derived exosomes and *miR-494-3p* regulate osteolytic tumor growth in the bone microenvironment, by injecting 4T1-Luc2 cells into the bone marrow cavity of the tibias of BALB/c mice. Quantification of the bioluminescence signal revealed that the exosome-treated mice exhibited an increased tumor growth in the tibia compared with the control mice, whereas exosome-induced tumor growth in the tibia was significantly suppressed by treatment with *miR-494-3p* inhibitor (Fig. 6C). Immunochemical staining of the tibiae revealed that the exosome-treated mice had a significantly increased number of TRAP-positive osteoclasts at the tumor-bone interface; however, treatment with *miR-494-3p* inhibitor reversed these effects (Fig. 6D). These results suggested that the exosome-mediated transfer of *miR-494-3p* from breast cancer cells to bone cells induced osteolytic bone metastases by stimulating osteoclastogenesis in the bone microenvironment.

Discussion

Understanding the molecular mechanisms underlying bone metastasis in breast cancer is critical for the development of novel strategies with which to treat and/or prevent bone metastasis. The present demonstrated that RAS activation in breast cancer cells stimulated the secretion of osteoclastogenic

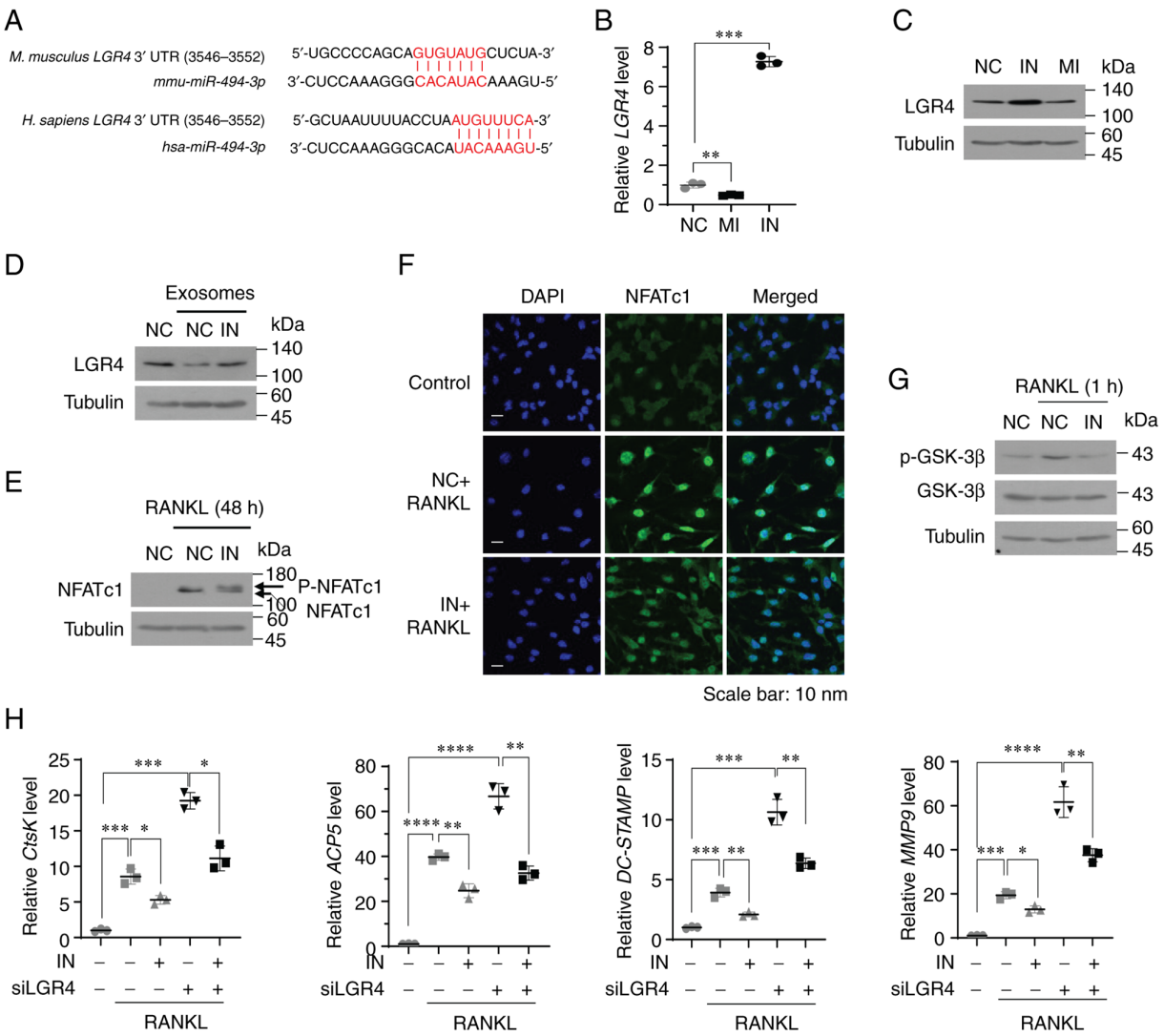

Figure 4. LGR4 is a potential target of miR-494-3p in osteoclasts. (A) *miR-494-3p* binding sites in human and murine *LGR4* mRNA. (B and C) RAW264.7 cells were transfected with miRNA negative control (NC), miR-494-3p mimic (MI, 20 nM), or miR-494-3p inhibitor (IN, 100 nM). The LGR4 mRNA (B) and protein (C) expression levels were determined using (B) RT-qPCR and (C) western blot analysis. (D) RAW264.7 cells were transfected with miRNA negative control miRNA (NC) or *miR-494-3p* inhibitor (IN, 100 nM) and subsequently incubated with exosomes ($3x10^7$ particles/ml) derived from MDA-MB-231 cells for 24 h. The expression level of LGR4 was determined using western blot analysis. (E) RAW264.7 cells were transfected with miRNA negative control miRNA (NC) or *miR-494-3p* inhibitor (IN, 100 nM) and subsequently stimulated with RANKL (100 ng/ml) for 48 h. The expression level of NFATc1 was determined using western blot analysis. (F) BMMs transfected with miRNA negative control miRNA (NC) or *miR-494-3p* inhibitor (IN, 100 nM) were stimulated with RANKL and M-CSF for 4 days. The cells were stained with an anti-NFATc1 antibody. DAPI was used to stain the nuclei. (G) RAW264.7 cells transfected with NC miRNA (NC) or *miR-494-3p* inhibitor (IN, 100 nM) were stimulated with RANKL for 1 h. The expression level of phospho-GSK-3β was determined using western blot analysis. (H) RAW264.7 cells transfected with *miR-494-3p* inhibitor (IN, 100 nM) and/or LGR4 siRNA (siLGR4) were stimulated with RANKL for 3 days. The expression levels of *CtsK, ACP5, DC-STAMP* and *MMP9* were determined using RT qPCR. *P<0.05, **P<0.01, ***P<0.001 and ****P<0.0001. RT-qPCR, reverse transcription-quantitative PCR; LGR4, leucine-rich repeat-containing G-protein coupled receptor 4; RANKL, receptor activator of nuclear factor-κB ligand; BMMs, bone marrow-derived macrophages; NFATc1, nuclear factor of activated T-cells 1; GSK-3β, glycogen synthase kinase 3β.

miR-494-3p, *miR-4508* and *miR-6869-5p* on exosomes to promote osteolytic bone metastasis. In addition, the functional role of exosomal *miR-494-3p* in remodeling the bone microenvironment to induce osteolytic bone metastasis *in vitro* and *in vivo* was described.

Breast cancer cells secrete various pro-osteoclastogenic factors, including interleukin (IL)-6, IL-1β, and parathyroid hormone-related protein, to activate osteoclast differentiation and function, triggering a vicious cycle in osteolytic bone metastasis (5,7,29). Accumulating evidence indicates that exosomes secreted by breast cancer cells participate in bone metastasis by enhancing osteoclast formation and function (14,30,31). miRNAs in exosomes may be critical mediators for generating a bone microenvironment suitable for tumor growth through crosstalk between cancer cells and the bone microenvironment (14,30-32). For example, it has been demonstrated that exosomal *miR-21* derived from SCP28 breast cancer cells contributes to pre-metastatic niche formation by transferring *miR-21* to osteoclasts, resulting in the promotion of osteolytic bone metastasis (31). *miR-20a-5p* derived from MDA-MB-231 cells also promotes the proliferation and differentiation of osteoclasts by targeting SRC kinase signaling inhibitor 1 (32). In the present study, RAS activation in breast cancer cells stimulated exosome-mediated osteoclastogenesis. In total, three *miRNAs-miR-494-3p, miR-4508* and *miR-6869-5p* were identified in exosomes as osteoclastogenic miRNAs whose

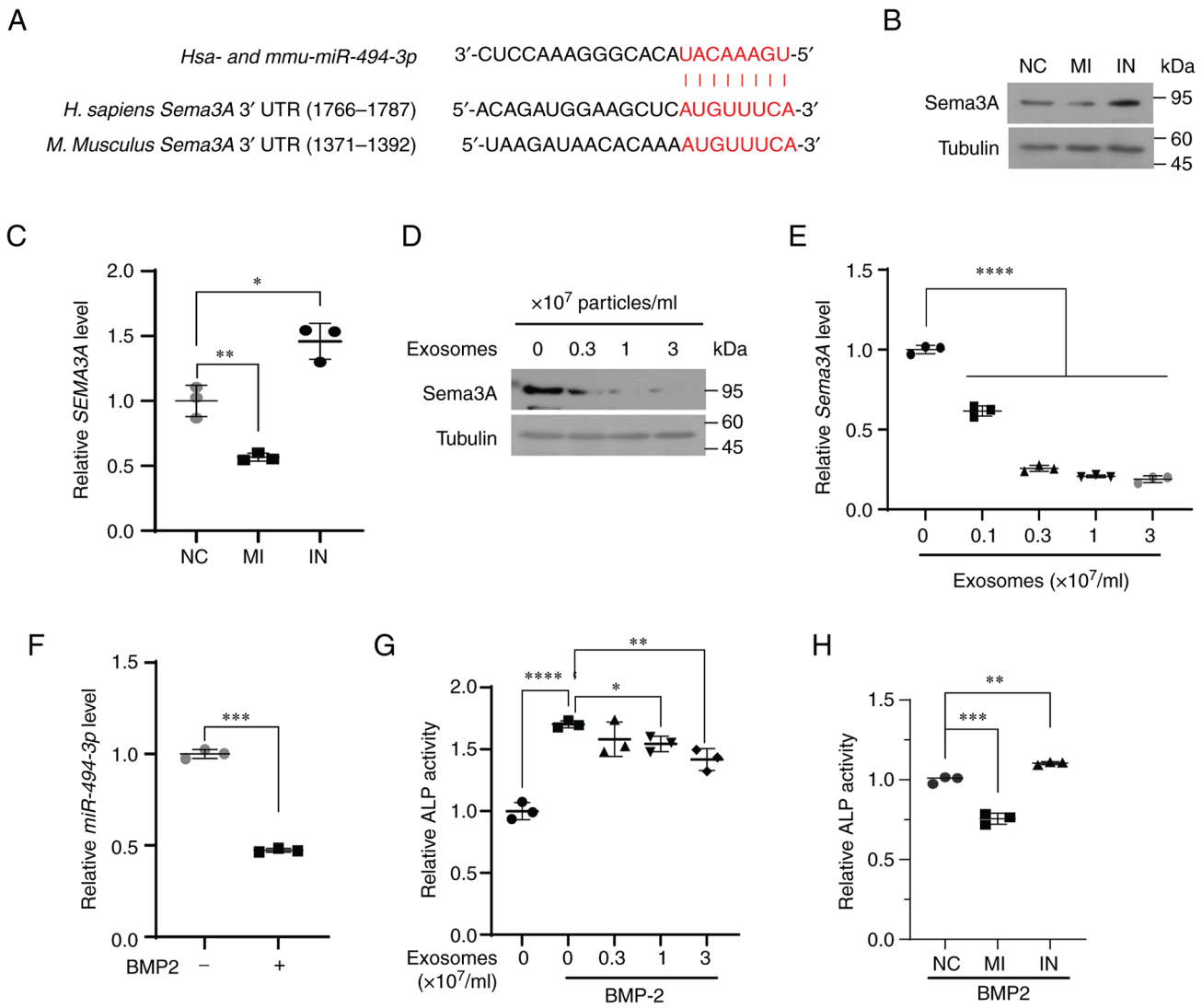

Figure 5. *SEMA3A* is a potential target of *miR-494-3p* in osteoblasts. (A) *miR-494-3p* binding sites in human and murine *SEMA3A* mRNA. (B and C) C2C12 cells were transfected with negative control miRNA (NC), *miR-494-3p* mimic (MI, 20 nM), or *miR-494-3p* inhibitor (IN, 100 nM). The expression level of SEMA3A was determined using (B) western blot analysis and (C) RT-qPCR. *P<0.05. (D and E) C2C12 cells were incubated with exosomes derived from MDA-MB-231 cells at the indicated concentrations for 24 h. The expression level of SEMA3A was determined using (D) western blot analysis and (E) RT-qPCR (n=3). ****P<0.0001. (F) The C2C12 cells were stimulated with BMP2 (30 ng/ml) for 3 days. The expression level of miR-494-3p was determined using RT-qPCR (n=3), ***P<0.001. (G) C2C12 cells incubated with exosomes derived from MDA-MB-231 cells at the indicated concentrations for 24 h were stimulated with BMP2 for 3 days. ALP activity was determined (n=3). *P<0.05, **P<0.01 and ****P<0.0001. (H) C2C12 cells transfected with NC miRNA (NC), *miR-494-3p* mimic (MI, 20 nM), and *miR-494-3p* inhibitor (IN, 100 nM) were incubated with BMP2 for 3 days. The activity of ALP was determined (n=3), **P<0.01 and ***P<0.001. SEMA3A, semaphorin 3A; RT-qPCR, reverse transcription-quantitative PCR; BMP2, bone morphogenetic protein 2; ALP, alkaline phosphatase.

expression increased upon RAS activation. *miR-494-3p* and *miR-1915-3p* suppressed BMP2-induced osteoblast differentiation. Notably, a *miR-494-3p* inhibitor suppressed the stimulatory effect of exosomes on RNAKL-induced osteoclastogenesis *in vitro* and the exosome-induced tumor growth in the tibia *in vivo*. These findings suggested that the activation of RAS signaling in breast cancer cells played an essential role in increasing the load of osteoclastogenic and anti-osteoblastogenic miRNAs, including *miR-494-3p* on exosomes.

Breast cancer is generally classified into four molecular subtypes based on the ER, PR and HER2 status: Luminal A (ER^+ and/or PR^+, $HER2^-$), luminal B (ER^+ and/or PR^+, $HER2^+$), HER2 (ER^- and/or PR^-, $HER2^+$) and basal-type (triple-negative) tumors (3). The bone is a common site of metastasis for all breast cancer subtypes, apart from basal-like tumors (4,33). The incidence of bone metastasis is highest in the luminal B subtype (4,33). In the present study, it was found that the levels of *miR-494-3p, miR-1915-3p*, *miR-4508* and *miR-6869-5p* in the serum of patients with HER2-positive human breast cancer were significantly higher than those in the serum of patients with triple-negative breast cancer. These findings indicated that the activation of RAS signaling via HER2 overexpression may induce osteolytic bone metastasis by increasing the release of osteoclastogenic and anti-osteoblastogenic miRNAs, including *miR-494-3p* from breast cancer cells in certain breast cancer subtypes, such as luminal B.

miR-494-3p is an onco-miRNA regulating cell proliferation, migration and invasion by targeting *PTEN*, *PTPN12*, or *SOX7* in different types of cancer cells (25,34-36). However, the functions of *miR-494-3p* in osteoclastogenesis and osteolytic bone metastasis remain unclear. In the present study, it was found that *miR-494-3p* promoted RANKL-induced

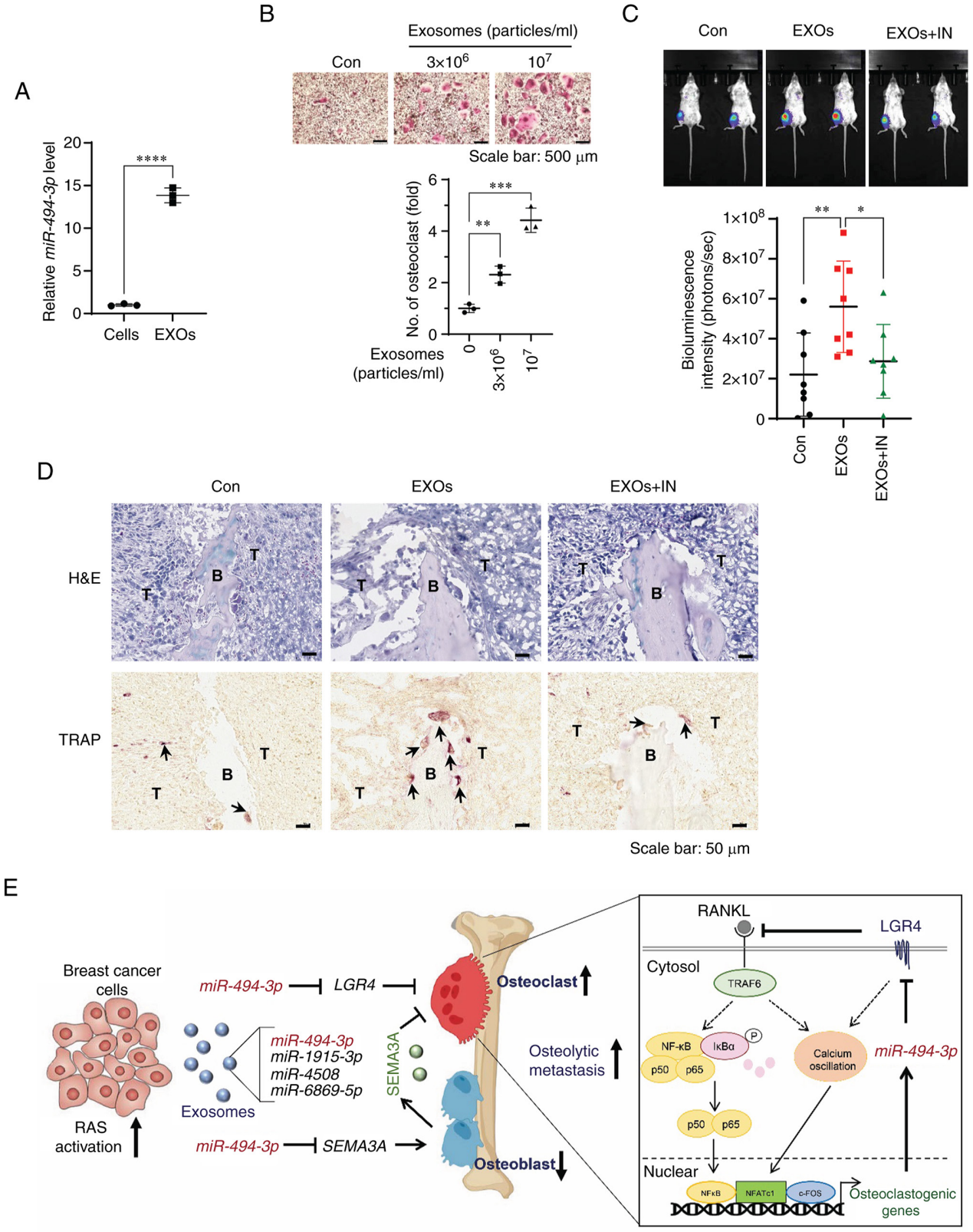

Figure 6. miR-494-3p inhibitor treatment suppresses the osteolytic bone metastasis of 4T1 breast cancer cells in a mouse model. (A) Expression levels of *miR-494-3p* in 4T1-Luc2 cells and exosomes (EXOs) derived from 4T1-Luc2 cells as determined using RT-qPCR. ****P<0.0001. (B) BMMs were treated with exosomes derived from 4T1-Luc2 cells in the presence of M-CSF and RANKL for 5 days. Representative images of TRAP staining. The graph represents the number of TRAP-positive multinucleated osteoclasts (n=3). Scale bar, 500 μm. **P<0.01 and ***P<0.001. (C) Representative bioluminescence images (upper panel) and quantification of bioluminescence intensity (lower panel) showing 4T1-Luc2 cell localization after 2 weeks in recipient mice with different treatments (n=8). Con, PBS treatment; EXOs, exosome treatment; EXOs + IN, exosomes puls *miR-494-3p* inhibitor treatment. *P<0.05 and **P<0.01. (D) Representative images of H&E and TRAP staining of bones isolated from the indicated mice on day 14 after exosomes (EXOs) or/and *miR-494-3p* inhibitor (IN) treatment. Arrows indicate TRAP-positive osteoclasts. B, bone; T, tumor. Scale bar, 50 μm. (E) Working model of exosomal *miR-494-3p* secreted from RAS-ativated breast cancer cells in regulating osteolytic bone metastasis of breast cancer cells. RANKL, receptor activator of nuclear factor-κB ligand; BMMs, bone marrow-derived macrophages; TRAP, tartrate-resistant acid phosphatase; H&E, hematoxylin and eosin; SEMA3A, semaphorin 3A; LGR4, leucine-rich repeat-containing G-protein coupled receptor 4.

osteoclastogenesis by targeting *LGR4* in osteoclast precursors, whereas it suppressed bone-forming osteoblast differentiation by targeting *SEMA3A*. In addition, treatment with *miR-494-3p* inhibitor suppressed exosome-mediated tumor growth and osteoclast formation in the tibia *in vivo*. These findings indicated that exosomal *miR-494-3p* secreted from breast cancer cells was a critical mediator of osteoclytic bone metastasis. LGR4 functions as a RANKL receptor that suppresses osteoclast differentiation and bone formation by activating Gαq-GSK-3β signaling pathway and inhibiting NF-κB activation, which results in the expression of and activity of NFATc1 during osteoclastogenesis (26). In the present study, treatment with *miR-494-3p* mimic downregulated LGR4 mRNA and protein expression, whereas that with *miR-494-3p* inhibitor reversed this effect in osteoclast precursors. Moreover, treatment with *miR-494-3p* inhibitor suppressed RANKL-induced activation of NF-κB and NFATc1, suggesting that *miR-494-3p* promoted osteoclast differentiation, at least in part, by targeting *LGR4*. SEMA3A regulates neuronal guidance, bone remodeling, cancer progression, and immune disorders (37). It is mainly expressed by osteoblasts, whereas its receptor, neuropilin 1, is expressed in osteoclast precursors (37). SEMA3A positively regulates osteoblast differentiation through the Wnt/β-catenin pathway, but suppresses osteoclast differentiation by suppressing phospholipase Cγ activation and calcium oscillation (27,28). Therefore, the findings presented herein suggested that *miR-494-3p* suppressed SEMA3A expression in osteoblast precursors, which may contribute to the stimulation of osteolytic bone lesion formation in the bone microenvironment.

In spite of these novel findings, the present study has several limitations. First, osteolytic bone metastasis *in vivo* is a complex process that is regulated by complex communications between cancer cells and stromal cells in the bone microenvironment. Moreover, a single miRNA can target multiple genes. The present study focused on the effects of *miR-494-3p* on osteoclastogenesis and osteoblastogenesis. Further studies are required to investigate other target genes of *miR-494-3p* in the bone microenvironment. Second, the present study only investigated the effects of *miR-494-3p* on osteolytic bone metastasis in female mice. Although male breast cancer is rare, it remains to be elucidated whether *miR-494-3p* may regulate osteolytic bone metastasis in male mice.

In conclusion, the present study found that RAS activation promoted exosome-mediated osteoclastogenesis by increasing the loading of osteoclastogenic miRNAs, including miR-494-3p, into exosomes. *miR-494-3p* is a major osteoclastogenic miRNA secreted by RAS-activated breast cancer cells. *miR-494-3p* promoted RANKL-induced osteoclastogenesis by targeting *LGR4* and *SEMA3A* in the bone microenvironment, and treatment with *miR-494-3p* inhibitor suppressed osteolytic lesions in an animal model. Overall, the results presented herein suggested that miRNAs in exosomes, including *miR-494-3p*, derived from RAS-activated breast cancer cells were critical mediators in the induction of osteolytic bone metastasis in human breast cancer.

Acknowledgements

The biospecimens and data used in the present study were provided by the Biobank of Kangwon University Hospital, a member of the Korea Biobank Network. The authors would like to acknowledge Professor Kwang-Yeol Lee, Chonnam National University, Republic of Korea, for the RAS constructs.

Funding

The present study was supported by grants from the National Research Foundation (NRF) of Korea (2020R1A5A8019180).

Availability of data and materials

The datasets used in the current study are available from the corresponding author on reasonable request. The original miRNA array data generated in the present study were submitted to the GEO repository (accession no. GSE235802). This accession no. is currently private and is scheduled to be released on June 16, 2024.

Authors' contributions

OK, PTT and MG performed the research. SJL and SHN contributed to the analyses of miRNAs in the serum of patients. CH analyzed the data. JHL designed the experiments and wrote the manuscript. OK, PTT and JHL confirm the authenticity of all the raw data. All authors have read and approved the final manuscript.

Ethics approval and consent to participate

All animal experimental protocols were approved by the Institutional Animal Care and Use Committee (IACUC) of Kangwon National University (KW-210914-1, September 23, 2021), and all experiments were performed in accordance with relevant regulation and guideline. Blood collection from breast cancer patients was performed following the guiding principles of the Declaration of Helsinki and was approved by the Institutional Review Board of Kangwon National University Hospital (KNUH-2022-04-011; approved date: May 4, 2022). The requirement for informed consent was waived by the Institutional Review Board of Kangwon National University Hospital owing to the retrospective nature of the study.

Patient consent for publication

Not applicable.

Competing interests

The authors declare that they have no competing interests.

References

1. Torre LA, Islami F, Siegel RL, Ward EM and Jemal A: Global cancer in women: Burden and trends. Cancer Epidemiol Biomarkers Prev 26: 444-457, 2017.
2. Hernandez RK, Wade SW, Reich A, Pirolli M, Liede A and Lyman GH: Incidence of bone metastases in patients with solid tumors: Analysis of oncology electronic medical records in the United States. BMC Cancer 18: 44, 2018.
3. Perou CM, Sørlie T, Eisen MB, van de Rijn M, Jeffrey SS, Rees CA, Pollack JR, Ross DT, Johnsen H, Akslen LA, *et al*: Molecular portraits of human breast tumours. Nature 406: 747-752, 2000.

4. Kennecke H, Yerushalmi R, Woods R, Cheang MC, Voduc D, Speers CH, Nielsen TO and Gelmon K: Metastatic behavior of breast cancer subtypes. J Clin Oncol 28: 3271-3277, 2010.
5. Coleman RE, Croucher PI, Padhani AR, Clézardin P, Chow E, Fallon M, Guise T, Colangeli S, Capanna R and Costa L: Bone metastases. Nat Rev Dis Primers 6: 83, 2020.
6. Waning DL and Guise TA: Molecular mechanisms of bone metastasis and associated muscle weakness. Clin Cancer Res 20: 3071-3077, 2014.
7. Weilbaecher KN, Guise TA and McCauley LK: Cancer to bone: A fatal attraction. Nat Rev Cancer 11: 411-425, 2011.
8. Wortzel I, Dror S, Kenific CM and Lyden D: Exosome-mediated metastasis: Communication from a distance. Dev Cell 49: 347-360, 2019.
9. Möller A and Lobb RJ: The evolving translational potential of small extracellular vesicles in cancer. Nat Rev Cancer 20: 697-709, 2020.
10. Théry C, Witwer KW, Aikawa E, Alcaraz MJ, Anderson JD, Andriantsitohaina R, Antoniou A, Arab T, Archer F, Atkin-Smith GK, *et al*: Minimal information for studies of extracellular vesicles 2018 (MISEV2018): A position statement of the international society for extracellular vesicles and update of the MISEV2014 guidelines. J Extracell Vesicles 7: 1535750, 2018.
11. Colombo M, Raposo G and Théry C: Biogenesis, secretion, and intercellular interactions of exosomes and other extracellular vesicles. Annu Rev Cell Dev Biol 30: 255-289, 2014.
12. Kalluri R and LeBleu VS: The biology, function, and biomedical applications of exosomes. Science 367: eaau6977, 2020.
13. Dai J, Su Y, Zhong S, Cong L, Liu B, Yang J, Tao Y, He Z, Chen C and Jiang Y: Exosomes: Key players in cancer and potential therapeutic strategy. Signal Transduct Target Ther 5: 145, 2020.
14. Wu M, Wang G, Hu W, Yao Y and Yu XF: Emerging roles and therapeutic value of exosomes in cancer metastasis. Mol Cancer 18: 53, 2019.
15. Lee TH, Chennakrishnaiah S, Audemard E, Montermini L, Meehan B and Rak J: Oncogenic ras-driven cancer cell vesiculation leads to emission of double-stranded DNA capable of interacting with target cells. Biochem Biophys Res Commun 451: 295-301, 2014.
16. Lobb RJ, Hastie ML, Norris EL, van Amerongen R, Gorman JJ and Möller A: Oncogenic transformation of lung cells results in distinct exosome protein profile similar to the cell of origin. Proteomics 17: 1600432, 2017.
17. Cha DJ, Franklin JL, Dou Y, Liu Q, Higginbotham JN, Demory Beckler M, Weaver AM, Vickers K, Prasad N, Levy S, *et al*: KRAS-dependent sorting of miRNA to exosomes. Elife 4: e07197, 2015.
18. McKenzie AJ, Hoshino D, Hong NH, Cha DJ, Franklin JL, Coffey RJ, Patton JG and Weaver AM: KRAS-MEK signaling controls Ago2 sorting into exosomes. Cell Rep 15: 978-987, 2016.
19. Rochlitz CF, Scott GK, Dodson JM, Liu E, Dollbaum C, Smith HS and Benz CC: Incidence of activating ras oncogene mutations associated with primary and metastatic human breast cancer. Cancer Res 49: 357-360, 1989.
20. Galiè M: RAS as supporting actor in breast cancer. Front Oncol 9: 1199, 2019.
21. Wright KL, Adams JR, Liu JC, Loch AJ, Wong RG, Jo CE, Beck LA, Santhanam DR, Weiss L, Mei X, *et al*: Ras signaling is a key determinant for metastatic dissemination and poor survival of luminal breast cancer patients. Cancer Res 75: 4960-4972, 2015.
22. Zheng ZY, Tian L, Bu W, Fan C, Gao X, Wang H, Liao YH, Li Y, Lewis MT, Edwards D, *et al*: Wild-type N-Ras, overexpressed in basal-like breast cancer, promotes tumor formation by inducing IL-8 secretion via JAK2 activation. Cell Rep 12: 511-524, 2015.
23. Banys-Paluchowski M, Milde-Langosch K, Fehm T, Witzel I, Oliveira-Ferrer L, Schmalfeldt B and Müller V: Clinical relevance of H-RAS, K-RAS, and N-RAS mRNA expression in primary breast cancer patients. Breast Cancer Res Treat 179: 403-414, 2020.
24. Gal M, Kim O, Tran PT, Huong LT, Nhiem NX, Van Kiem P, Dang NH and Lee JH: Mussaendoside O, a N-triterpene cycloartane saponin, attenuates RANKL-induced osteoclastogenesis and inhibits lipopolysaccharide-induced bone loss. Phytomedicine 105: 154378, 2022.
25. Kim O, Hwangbo C, Tran PT and Lee JH: Syntenin-1-mediated small extracellular vesicles promotes cell growth, migration, and angiogenesis by increasing onco-miRNAs secretion in lung cancer cells. Cell Death Dis 13: 122, 2022.
26. Luo J, Yang Z, Ma Y, Yue Z, Lin H, Qu G, Huang J, Dai W, Li C, Zheng C, *et al*: LGR4 is a receptor for RANKL and negatively regulates osteoclast differentiation and bone resorption. Nat Med 22: 539-546, 2016.
27. Hayashi M, Nakashima T, Taniguchi M, Kodama T, Kumanogoh A and Takayanagi H: Osteoprotection by semaphorin 3A. Nature 485: 69-74, 2012.
28. Li Z, Hao J, Duan X, Wu N, Zhou Z, Yang F, Li J, Zhao Z and Huang S: The role of semaphorin 3A in bone remodeling. Front Cell Neurosci 11: 40, 2017.
29. Mundy GR: Metastasis to bone: Causes, consequences and therapeutic opportunities. Nat Rev Cancer 2: 584-593, 2002.
30. Jabbari N, Akbariazar E, Feqhhi M, Rahbarghazi R and Rezaie J: Breast cancer-derived exosomes: Tumor progression and therapeutic agents. J Cell Physiol 235: 6345-6356, 2020.
31. Yuan X, Qian N, Ling S, Li Y, Sun W, Li J, Du R, Zhong G, Liu C, Yu G, *et al*: Breast cancer exosomes contribute to pre-metastatic niche formation and promote bone metastasis of tumor cells. Theranostics 11: 1429-1445, 2021.
32. Guo L, Zhu Y, Li L, Zhou S, Yin G, Yu G and Cui H: Breast cancer cell-derived exosomal miR-20a-5p promotes the proliferation and differentiation of osteoclasts by targeting SRCIN1. Cancer Med 8: 5687-5701, 2019.
33. Arciero CA, Guo Y, Jiang R, Behera M, O'Regan R and Peng L and Li X: ER+/HER2+ breast cancer has different metastatic patterns and better survival than ER-/HER2+ breast cancer. Clin Breast Cancer 19: 236-245, 2019.
34. Faversani A, Amatori S, Augello C, Colombo F, Porretti L, Fanelli M, Ferrero S, Palleschi A, Pelicci PG, Belloni E, *et al*: miR-494-3p is a novel tumor driver of lung carcinogenesis. Oncotarget 8: 7231-7247, 2017.
35. Wu C, Yang J, Li R, Lin X, Wu J and Wu J: LncRNA WT1-AS/miR-494-3p regulates cell proliferation, apoptosis, migration and invasion via PTEN/PI3K/AKT signaling pathway in non-small cell lung cancer. Onco Targets Ther 14: 891-904, 2021.
36. He H, Liao X, Yang Q, Liu Y, Peng Y, Zhong H, Yang J, Zhang H, Yu Z, Zuo Y, *et al*: MicroRNA-494-3p promotes cell growth, migration, and invasion of nasopharyngeal carcinoma by targeting Sox7. Technol Cancer Res Treat 17: 1533033818809993, 2018.
37. Behar O, Golden JA, Mashimo H, Schoen FJ and Fishman MC: Semaphorin III is needed for normal patterning and growth of nerves, bones and heart. Nature 383: 525-528, 1996.